# Supporting Information

# Design flower-like C-$MnO_2$ nanosheets on carbon cloth: toward high-performance flexible zinc-ion batteries

Fei Li[1,†], Yi-Lin Liu[1,†], Gui-Gen Wang*[,†], Dong Yan[††], Gui-Zhong Li[†], Hai-Xu Zhao[†], Hua-Yu Zhang*[,†], Hui-Ying Yang*[††]

[†]*Shenzhen Key Laboratory for Advanced Materials, School of Materials Science and Engineering, Harbin Institute of Technology, Shenzhen, Shenzhen 518055, China*

[††]*Pillar of Engineering Product Development, Singapore University of Technology and Design, 8 Somapah Road, Singapore 487372, Singapore*

*Corresponding Authors:*

*(Gui-Gen Wang) wangguigen@hit.edu.cn;*

*(Hua-Yu Zhang) hyzhang@hit.edu.cn;*

*(Hui Ying Yang) yanghuiying@sutd.edu.sg*

*1 These two authors contributed equally to this work.*

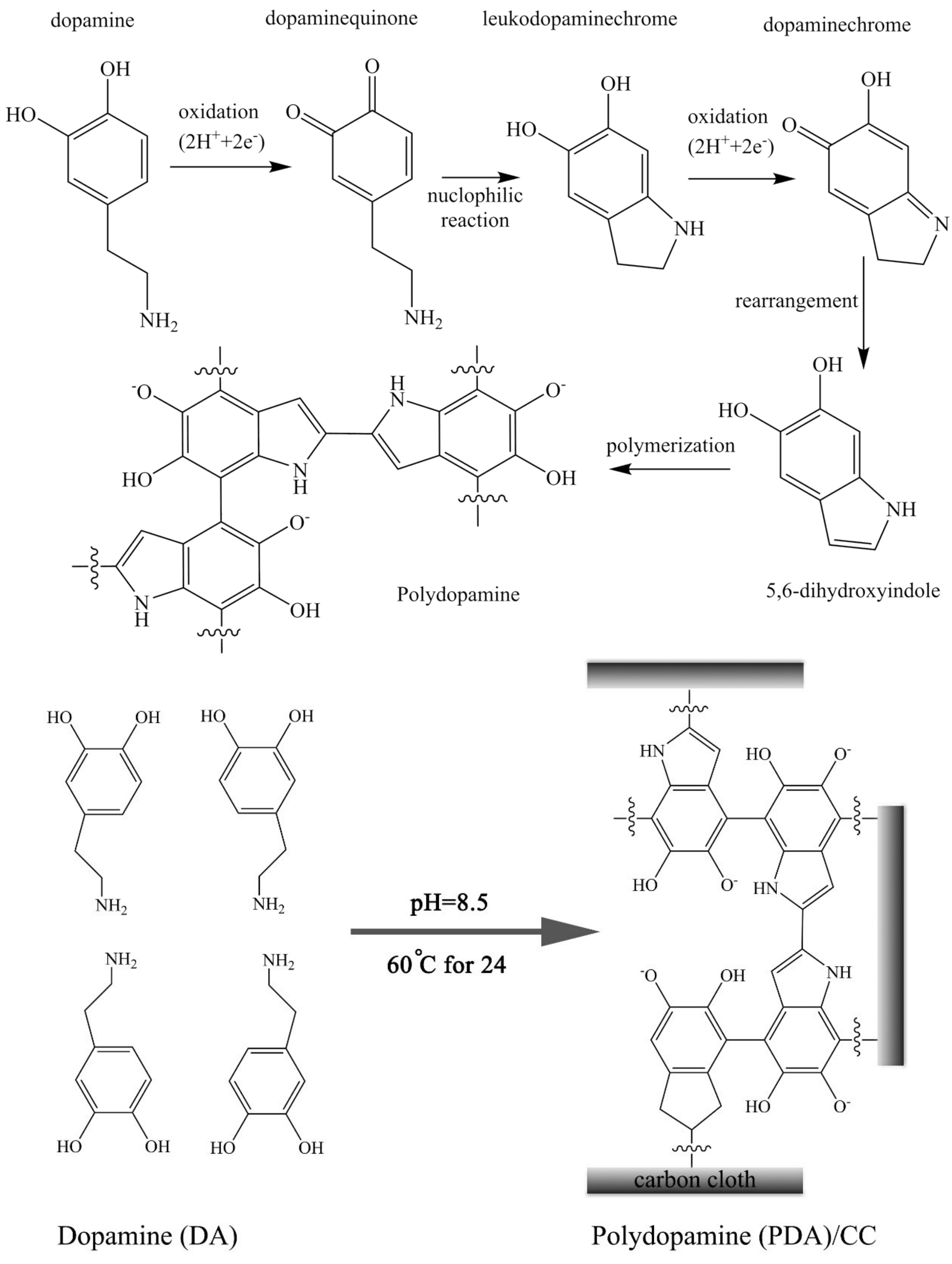


**Fig. S1** Self-polymerization of dopamine (DA) on carbon cloth (CC) with the chemical equation.

Under oxidation condition, e.g. alkaline pH, dihydroxyl group protons in dopamine are deprotonated, becoming dopamine-quinone, which subsequently rearranges via intramolecular cyclization to the formation of leukodopaminechrome. Further oxidation and rearrangement leads to 5,6-dihydroxyindole, which further oxidation causes inter-molcular cross-linking to yield a polymer that have similar structure with the bio-pigment melanin. The polydopamine-coated surface subsequently reacts with a variety of molecules via Shiff-base and Michael addition chemistries [1-3].

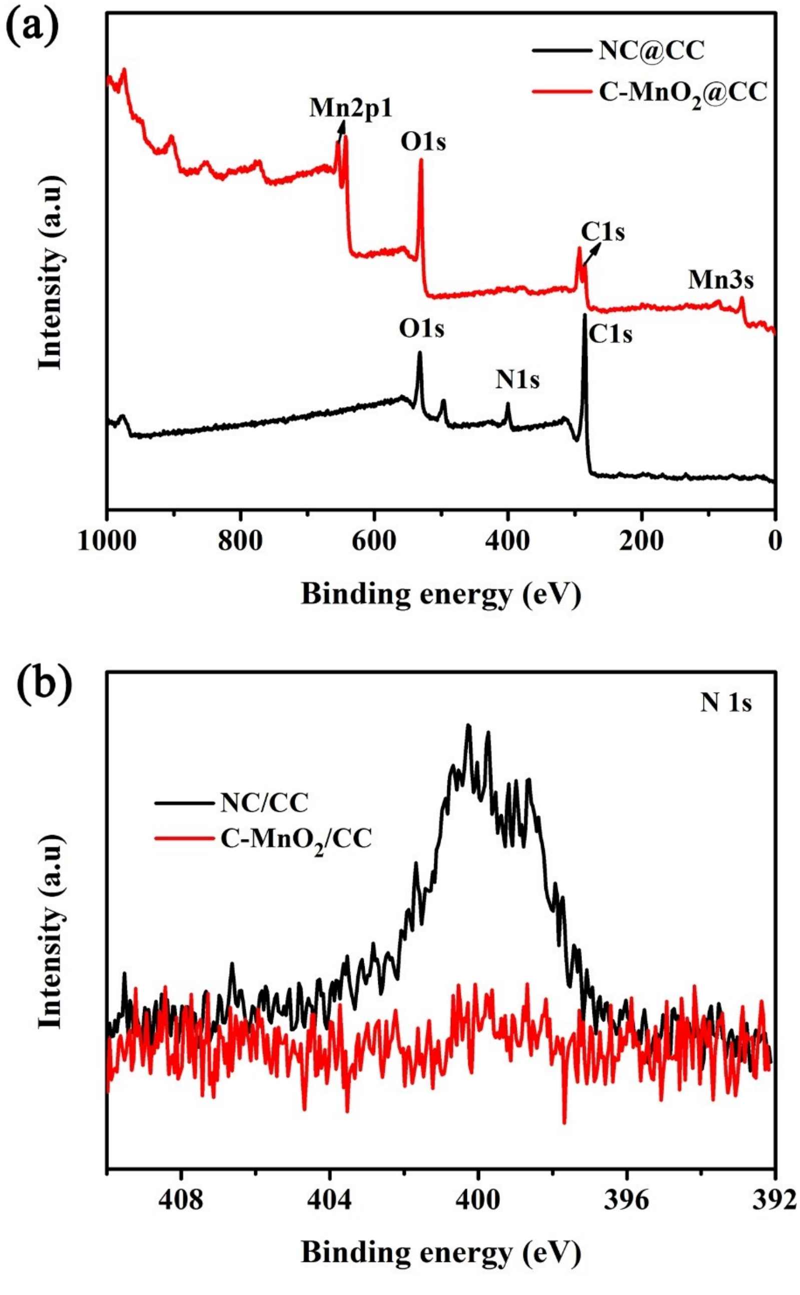


**Fig. S2** XPS spectra of C-$MnO_2$/CC electode materials: (a) XPS survey spectra, (b) High-resolution XPS spectra of N 1s.

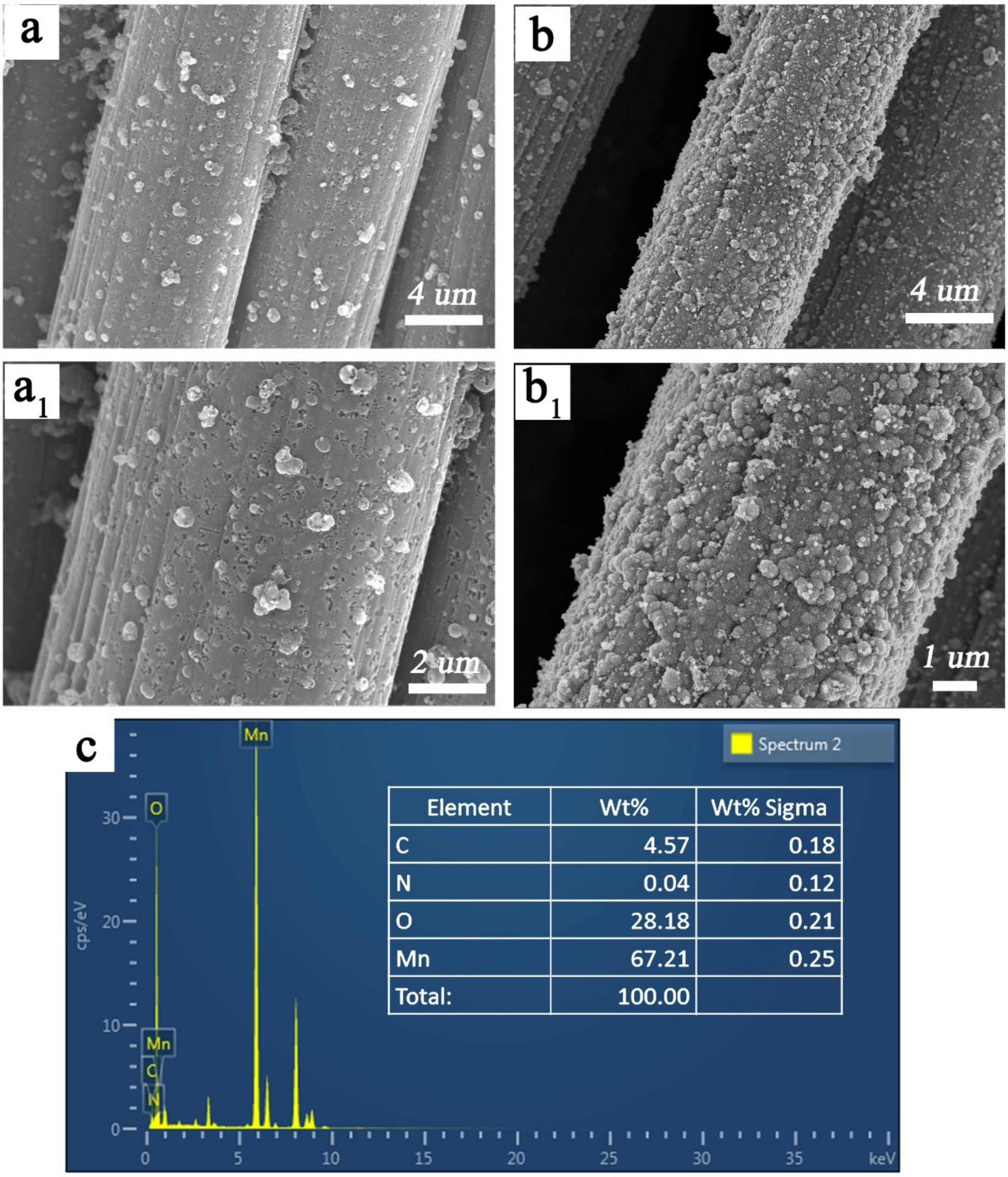


**Fig. S3** SEM images of NC-CC (a, a1) and C-$MnO_2$/CC (b, b1), (c) EDS spectrum of C-$MnO_2$ with the elemental composition at TEM pattern.

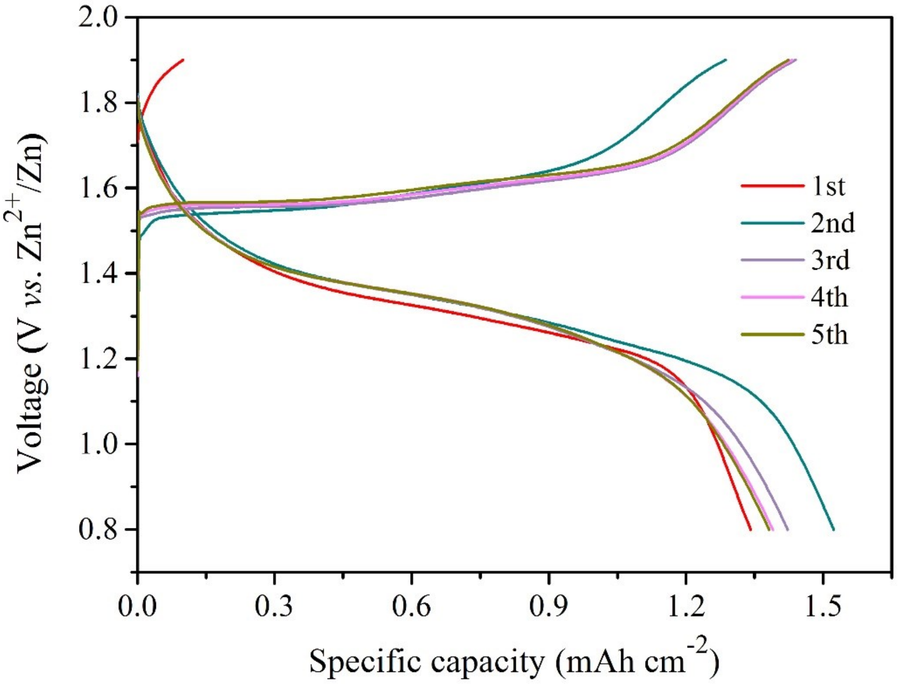


**Fig. S4** The initial five cyclic GCD curves of C-$MnO_2$/CC at current density of 1.0 mA $cm^{-2}$.

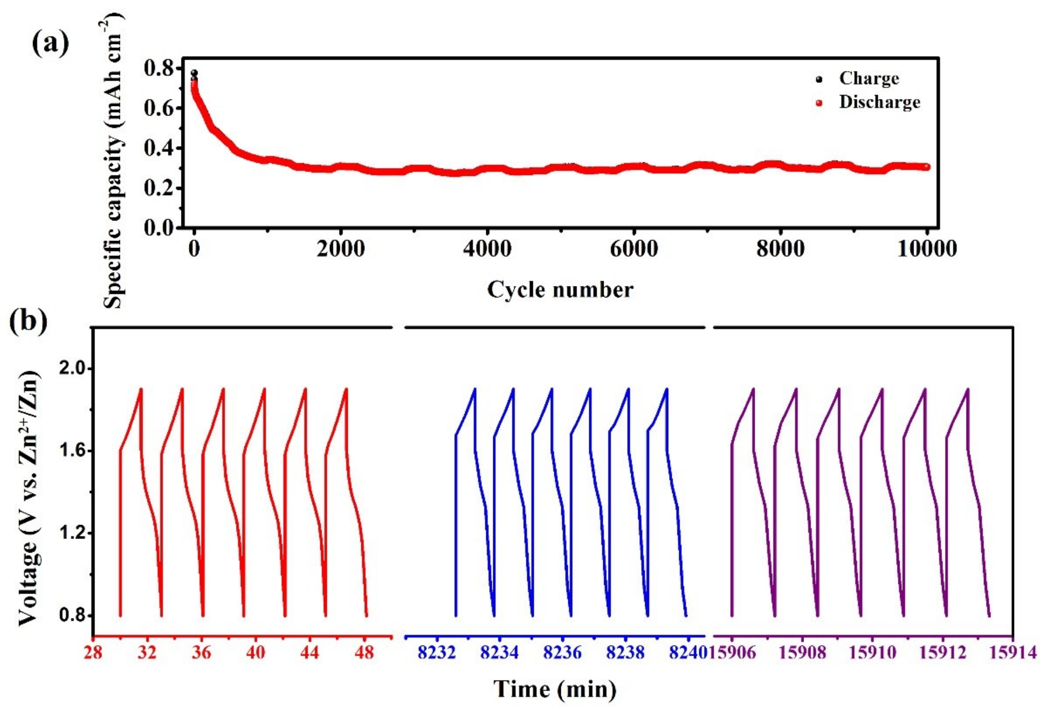


**Fig. S5** Cycling test of Zn//C-$MnO_2$ battery at 10 mA $cm^{-1}$: (a) The long-term cycling stability, (b) GCD curves of 45~50 cycles, 4995~5000 cycles, and 9995~10000 cycles.

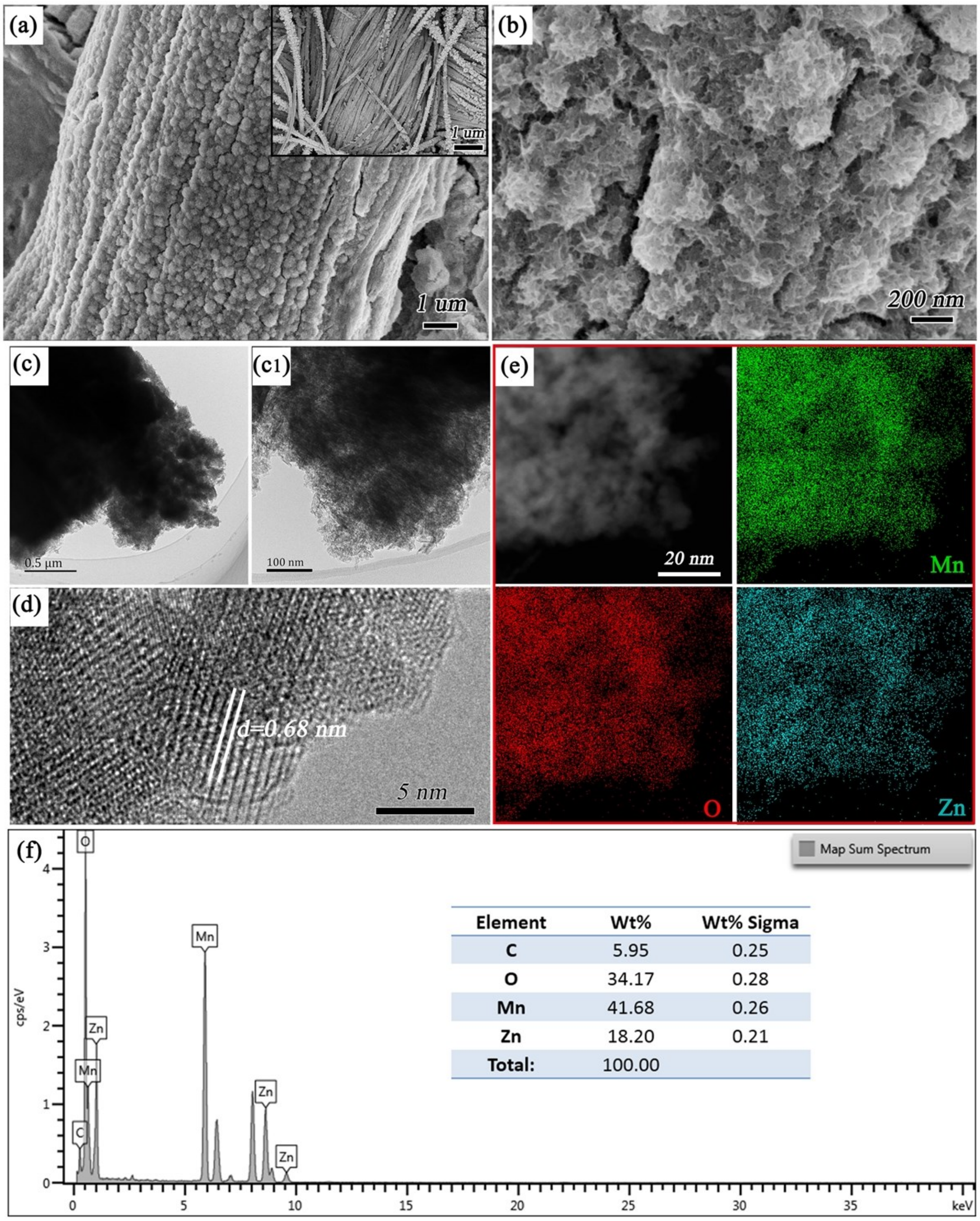


**Fig. S6** The SEM and TEM images of C-$MnO_2$@CC after cycling for 10000 times. As the SEM images of C-$MnO_2$@CC (a) with different magnifications (b) shown that C-$MnO_2$ still tight cover on the carbon fibre with less fall off and keep the “flower-like” nanosheet-like morphology; TEM images (c-c1) and HRTEM images (d) further confirm the $MnO_2$ retain nanosheet structure and 0.68 nm of lattice spacing; (e) Selected-area elemental mappings of Mn, O, and Zn displays that the $Zn^{2+}$ insert into the $MnO_2$ and uniform distribution. (f) EDS spectra of C-$MnO_2$ with the elemental compositions at TEM pattern reveals that the content of C, O, Mn, and Zn is 5.95, 34.17, 41.68, and 18.2 *wt*%, respectively.

**Table S1.** Comparison of flexible $MnO_2$ cathodes for zinc ion batteries.

| Electrode | Electrolyte | Specific capacity | Current density | Reference |
|---|---|---|---|---|
| N-CNSs@$MnO_2$//N-CNSs@Zn battery | 2 M $ZnSO_4$ + 0.2 M $MnSO_4$ | 0.698 mAh $cm^{-2}$ | 0.46 mA $cm^{-2}$ (2.3 mg $cm^{-2}$; 0.2 A $g^{-1}$) | *Energy Storage Materials*. **2020**, 29, 52-59 |
| polyester-CNTs@$MnO_2$// Zn-CNTs battery | 2 M $ZnSO_4$ + 0.2 M $MnSO_4$ | 0.96 mAh $cm^{-2}$ | 1 mA $cm^{-2}$ (1.9 mg cm-2) | *Advanced Energy Materials*. **2019**, *9*, 1901469 |
| Na:$MnO_2$/GCF//Zn/GCF battery | 2 M $ZnSO_4$ + 0.1 M $MnSO_4$ | 0.573 mAh $cm^{-2}$ | 0.15 mA $cm^{-2}$ (1.5 mg $cm^{-2}$; 0.1 A $g^{-1}$) | *Adv. Functional. Materials*. **2020**, *30*, 1907120 |
| Zn*x*$MnO_2$//ACC Zn-HSCs | 2 M $ZnSO_4$ + 0.4 M $MnSO_4$ | 0.97 mAh $cm^{-2}$ | 2 mA $cm^{-2}$ | *Small*, **2020**, 2000091. |
| $MnO_2$/Zn battery | 2 M $ZnSO_4$ + 0.1 M $MnSO_4$ | 1.1 mAh $cm^{-2}$ | 1.5 mA $cm^{-2}$ (5 mg $cm^{-2}$) | *Advanced Science*. **2020**, *7*, 1902795 |
| P-$MnO_{2-x}$@VMG//Zn@VMG battery | 2 M $ZnSO_4$ + 0.2 M $MnSO_4$ | 1.24 mAh $cm^{-2}$ | 2 mA $cm^{-2}$ (4.1 mg $cm^{-2}$; 0.5 A $g^{-1}$) | *Small Methods,* **2020**, 1900828 |
| quasi-solid-state Zn-CMOP ($MnO_2$/PEDOT) device | 2 M $ZnCl_2$ + 0.4 M $MnSO_4$ | 1.1 mAh $cm^{-2}$ | 2 mA $cm^{-2}$ (3 mg $cm^{-2}$) | *Small Methods* **2019**, *3*, 1900525 |
| OD-ZMO//Zn and OD-ZMO@PEDOT //Zn battery | 1 M $ZnSO_4$ | 1.05 mAh $cm^{-2}$ 1.37 mAh $cm^{-2}$ | 0.5 mA $cm^{-2}$ (6 mg $cm^{-2}$; 6.2 mg $cm^{-2}$) | *Energy Storage Materials*. **2019**, 21, 154-161 |
| Zn-δ-NMOH//Zn/CC | 2 M $ZnCl_2$ + 0.2 M $MnSO_4$ | 1.43 mAh $cm^{-2}$ | 1.0 mA $cm^{-2}$ (2~3 mg $cm^{-2}$; 0.380 A $g^{-1}$) | *ACS Nano*. **2019**, 13, 10643-10652 |
| $MnO_2$@PEDOT// Zn device | 1 M $Zn(NO_3)_2$ + 0.1 M $MnSO_4$ | 1.02 mAh $cm^{-2}$ | 2 mA $cm^{-2}$ (3.6 mg $cm^{-2}$; 0.37 A $g^{-1}$) | *Advanced Materials*. **2017**, *29*, 1700274 |
| N-CC@$MnO_2$//N-CC@Zn | 2 M $ZnCl_2$+0.4 M | | 1.6 mA $cm^{-2}$ | Journal of Materials |

| | | | | |
|---|---|---|---|---|
| | | | 0.5 A $g^{-1}$) | Chemistry A. **2017**, 5, 14838-14846 |
| $C-MnO_2/CC//Zn$ battery and $C-MnO_2/CC//Zn/CC$ device | 2 M $ZnSO_4$ + 0.2 M $MnSO_4$ | 1.3 mAh $cm^{-2}$ and 0.98 mAh $cm^{-2}$ | 1 mA $cm^{-2}$ (5 mg $cm^{-2}$) | This work |

**Table S2.** The Rs and Rp value at of the $Zn//C-MnO_2$ batteries at different state corresponding to Fig. 2e.

| Batteries | Rs (Ω) | Rp (Ω) |
|---|---|---|
| Pristine | 15.88 | 44.51 |
| 10 cycles | 14.5 | 50.18 |
| 50 cycles | 13.9 | 54.15 |
| 100 cycles | 12.69 | 36.81 |

The ion diffusion coefficient was calculated based on the following equation:

$D = R^2 \cdot T^2/(2 \cdot A^2 \cdots\cdots n^4 \cdot F^{\cdot 4} m^2 \cdot \sigma^2)$

where $D$ is the diffusion coefficient, $R$ is the gas constant, $T$ is the room temperature, $A$ is the surface area of the electrode, $n$ is the number of the electrons per molecule attending the electronic transfer reaction, $F$ is the Faraday constant, $m$ is the concentration of insertion ion in the $MnO_2$, and σ is the Warburg factor obtained from the fitted slope of the line $Z'$-$\omega^{-1/2}$. The resulted $D$ were $3.85\times10^{-13}$ $cm^2$ $s^{-1}$, $1.50\times10^{-12}$ $cm^2$ $s^{-1}$, $9.38\times10^{-13}$ $cm^2$ $s^{-1}$ and $1.86\times10^{-12}$ $cm^2$ $s^{-1}$ for the pristine, 10th , 50th, and 100th discharge stage, respectively.

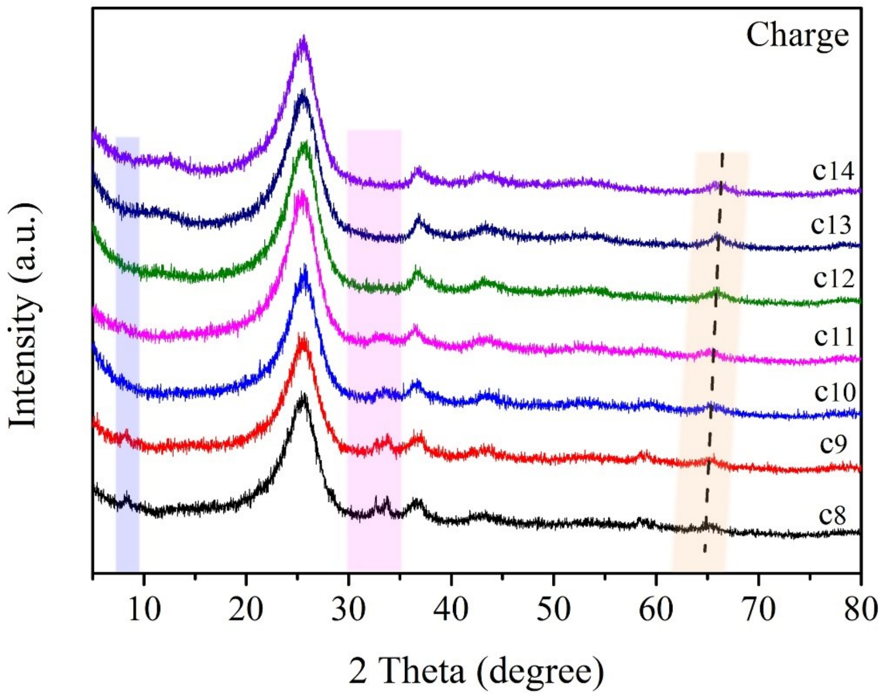


**Fig. S7** The ex-situ XRD patterns of C-$MnO_2$ electrode under charging process.

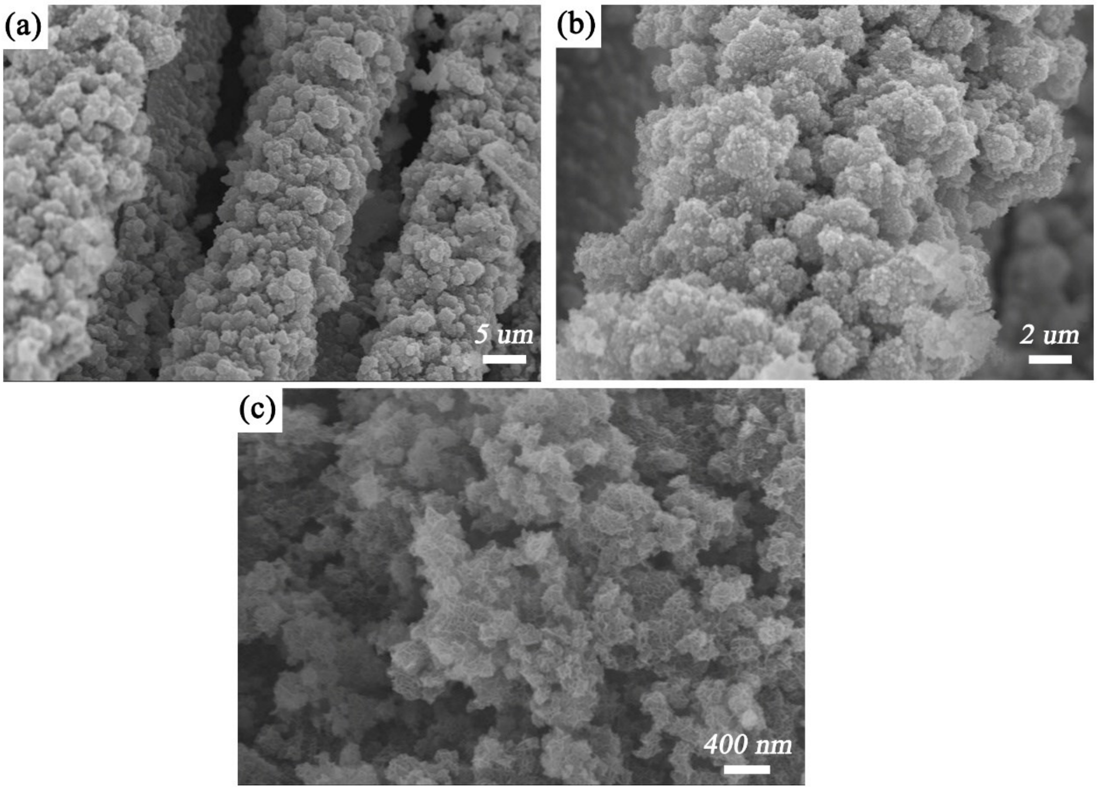


**Fig. S8** SEM images of C-$MnO_2$ electrode at d8 state with different magnifications.

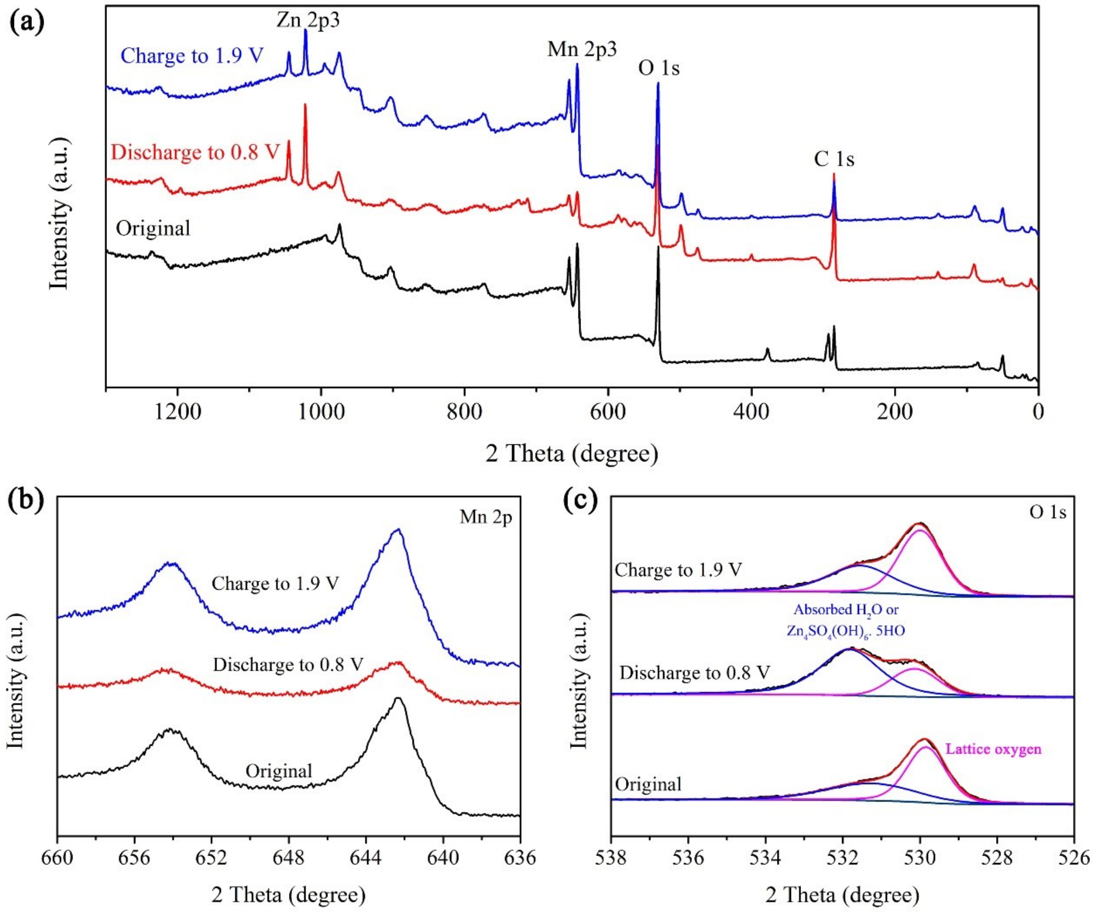


**Fig. S9** XPS of C-$MnO_2$@CC electrode materials at original, full discharge (0.8 eV), and full charge (1.9 eV): (a) XPS survey spectra. High-resolution XPS spectra of Mn 2p (b) and O 1s (c).

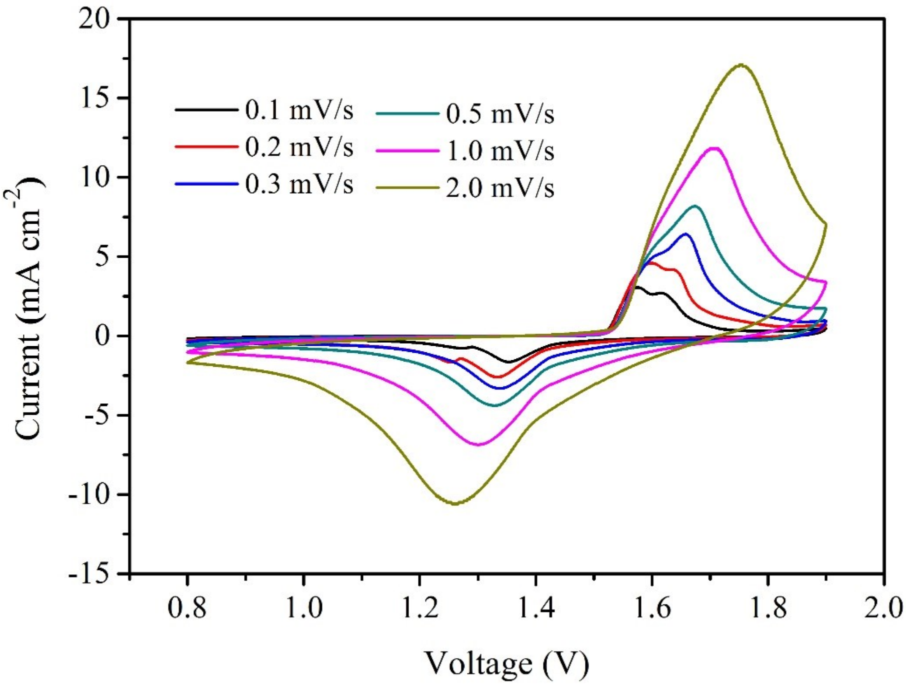


**Fig. S10** CV curves of flexible quasi-solid-state C-$MnO_2$@CC//Zn/CC batteries at different scan rates from 0.1 to 2.0 mV $s^{-1}$.

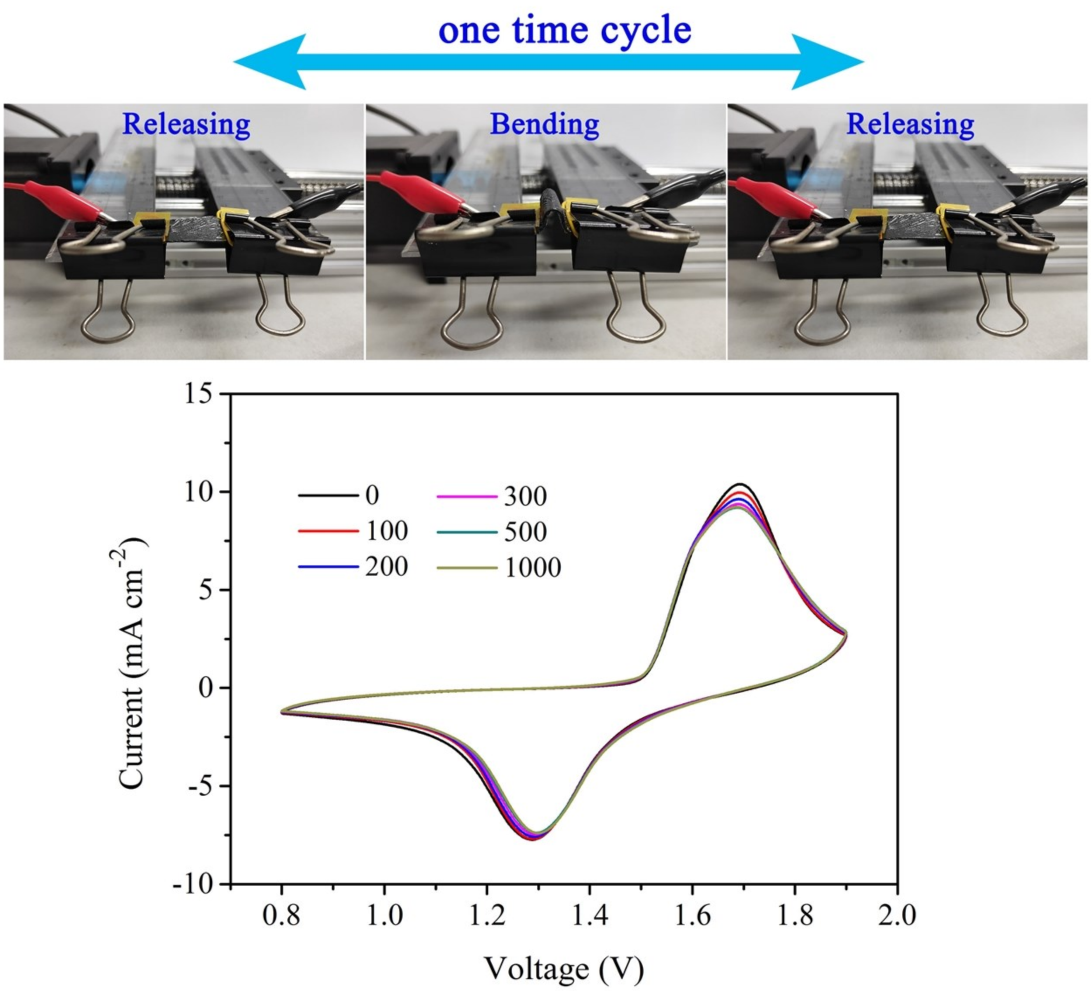


**Fig. S11** CV curves of the C-$MnO_2$@CC//Zn/CC device collected at a scan rate of 1 mV $s^{-1}$, in which the device were bended and then released after 100, 200, 300, 500, and 1000 times. There are digital photographs during one cycle.

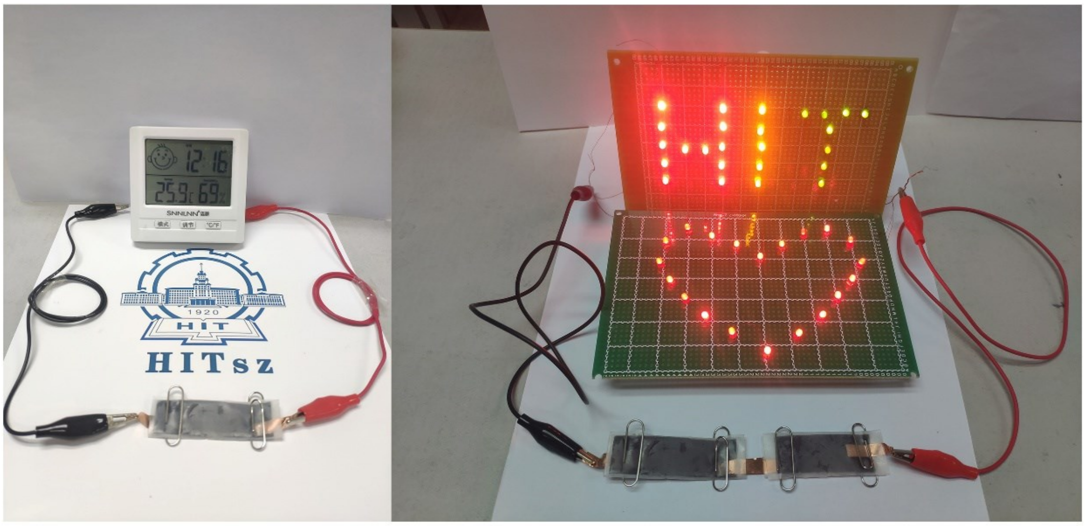


**Fig. S12** Flexible C-$MnO_2$@CC zinc ion battery and its application, and photographs of the digital watch and LED-designed pattern powered by our batteries.

Reference:

[1] Lee H , Dellatore S M , Miller W M , et al. Mussel-Inspired Surface Chemistry for Multifunctional Coatings [J]. Science, 2007, 318(5849):426-430.

[2] Hong S, Na Y S, Choi S, et al. Non-Covalent Self-Assembly and Covalent Polymerization Co-Contribute to Polydopamine Formation [J]. Advanced Functional Materials, 2012, 22(22):4711-4717.

[3] Liu Y, Ai K, Lu L. Polydopamine and Its Derivative Materials: Synthesis and Promising Applications in Energy, Environmental, and Biomedical Fields [J]. Chemical Reviews, 2014, 114(9):5057-5115.